



Microstructure and Properties of Casting Fe–Cr–B Alloy After Quenching Treatment

Tian Ye¹ · Fu Hanguang¹  · Lin Jian¹ · Guo Xingye¹ · Lei Yongping¹

Received: 15 September 2018 / Accepted: 14 March 2019 / Published online: 5 April 2019
© The Indian Institute of Metals - IIM 2019

Abstract The as-cast microstructure of Fe–4Cr–B alloy has been systematically investigated, which contains 1 wt%B, 4 wt%Cr, 0.35 wt%C, 0.8 wt%Si and 0.8 wt%Mn. The investigation was carried out by optical microscopy (OM), scanning electron microscopy (EDS/SEM), X-ray diffraction (XRD), hardness tester and wear tester, and the quenching temperature effect on its microstructure and mechanical property was studied. The results showed that ferrite, pearlite, martensite and borocarbides were the main composition of the solidification microstructure of casting Fe–4Cr–B alloy. After water quenching at 950–1150 °C, the matrix transformed to martensite, and the secondary borocarbides $M_{23}(C, B)_6$ precipitated from the matrix, and then the continuous distribution of $M_2(B, C)$ ($M = Fe, Cr, Mn$) among dendrites began to break. As the water quenching temperature increased, the phenomenon of disconnection became more clearly. When the water quenching temperature was 1100 °C, the network borocarbides fractured and formed an isolated distribution. The hardness of the alloy increased first and then decreased. At water quenching temperature of 1100 °C, the hardness reached the maximum of 62.8 HRC. The abrasive resistance and hardness of casting Fe–4Cr–B alloy changed at the same trend.

Keywords Abrasive resistance · Hardness · Microstructure · Quenching temperature · Casting Fe–4Cr–B alloy

1 Introduction

As a failure mode of mechanical equipment, wear failure causes a lot of economic losses every year. A lot of researches about how to reduce the loss caused by material wear have been done by many scholars [1–3]. More work has been done on the related research of the third-generation wear-resistant material high-chromium cast iron [4]. Because high-chromium cast iron has a tendency to deform or crack during high-temperature heat treatment, it is usually necessary to add alloy elements to improve the hardenability of the castings. The study has shown [5] that the impact toughness shows an obvious increase (about 50%); when the addition of cerium is 0.5 wt%, the impact toughness is improved obviously compared with specimen without alloy element. And the addition of Mn, Mo, Ni and Cu can increase the hardenability of high-chromium cast iron, the high alloying elements content increases the production cost, and in the case of increasing shortage of mineral resources, the long-term development of high-chromium cast iron is inhibited [5, 6]. In recent years, more and more researches have been carried out on new Fe–Cr–B wear-resistant alloys, the rockwell hardness of Fe–Cr–B alloy containing 0.35% C, 12% Cr and 1.4% B reaches 65.7 HRC, the borocarbide is $(Cr, Fe)_7(C, B)_3$, and the boride is Fe_2B as wear-resistant skeleton [7]. Under non-equilibrium conditions (i.e., under real conditions), the statistical model established by Christodoulou and Calos [8] shows that during the solidification of Fe–Cr–B alloy, the liquid

✉ Fu Hanguang
hgfu@bjut.edu.cn; fhg64@263.net

¹ School of Materials Science and Engineering, Beijing University of Technology, Number 100, Pingle Garden, Chaoyang District, Beijing 100124, People's Republic of China

phase first crystallizes into the matrix phase, and the remaining material solidifies in the form of eutectic. Based on the conclusions of the statistical model, they predicted that the change in chemical composition ranges to 0.11–1.05 wt%C, 3.85–19.5 wt%Cr, 0.01–2.75 wt%B, 0.29–1.22 wt%Si, 0.24–1.25 wt%Mn, 0.09–2.32 wt%Ni, 0.01–2.00 wt%Cu and 0–0.51 wt%Mo [8]. This is an important reference for designing the chemical composition of Fe–Cr–B alloy. Zhang et al. [9–11] made a series of researches on the abrasive resistance of casting Fe–B alloy, and they compared the relative hardness (the ratio of hardness of material to hardness of abrasive) between the samples with different Cr contents and as-quenched high-chromium cast iron (Cr15), and the results show that its wear resistance is twice than that of the Cr15 white cast iron. Casting Fe–Cr–B alloy develops based on the boron-bearing high-chromium white cast iron and high-chromium cast steel, which has better hardenability than the commonly used Cr20 white cast iron [12]. It has been found that Fe–Cr–B alloy has good wear resistance and thermal shock resistance [13].

Christodoulou et al. [8] found that the as-cast Fe–Cr–B alloy was heated at 1050 °C for 2 h, and after air cooling, the phase composition was analyzed: mainly (Fe, Cr)₂B, (Fe, Cr)₃(C, B), (Fe, Cr)₅(C, B)₂, (Fe, Cr)₇(C, B)₃, (Fe, Cr)₂₃(C, B) and martensite. A small amount of retained austenite was also found. Because heat treatment can change the types of phases of matrix and eutectic borocarbides, the morphology, quantity and distribution of eutectic borocarbides can also be affected, and after quenching, the matrix transforms into martensite to increase the hardness and wear resistance of the alloy. And with different heat treatment methods, the hardness and wear resistance of alloy improves at different degrees. This paper studies the influence mechanism of water quenching temperature on mechanical properties and microstructure of casting Fe–Cr–B alloy, and the quantitative relationship between transitions between eutectic phases and changing rules are analyzed. It is hoped that the present study can provide the practical way of producing cast Fe–Cr–B alloy with guidance for the selection of quenching parameters to control the microstructure and quantification of hard phases of the alloy.

2 Experimental Procedure

2.1 Experimental Materials

A vacuum induction furnace (10 kg) was used to melt the Fe–Cr–B alloy with scrap steel, ferrobore, ferrosilicon, ferrochromium, manganese and carburizer as raw materials. After the compositions were adjusted and qualified, the

molten steel temperature was raised to about 1600 °C, the molten steel got melted and deoxidized by adding aluminum, and then, the slag was stripped out of the furnace. The liquid steel was super-heated to 1610 °C, then poured into a ϕ 60 mm \times 220 mm cylindrical ingot in cast iron mold at 1520 °C, and then air-cooled to room temperature 25 °C. The samples of 12.5 mm \times 19 mm \times 12.5 mm were cut in the lower part of the ingot by wire-cutting machinery. Fe–Cr–B alloy is iron-based material, and the design chemical composition of it is 0.35C–4Cr–1.0B–0.8Mn–0.8Si–0.03P–0.03S (wt%). Some of the as-cast specimens were heat-treated in a conventional box-type resistance furnace at 950–1150 °C for 1 h, followed by water cooling to room temperature 25 °C. The samples were ground by sandpaper with 200#, 400#, 600#, 800#, 1000#, 1500# and 2000#, polished, alcohol cleaned and were allowed to corrode. The corrosion solution was 4% CuSO₄ solution. After corrosion, the samples were washed and dried with alcohol.

2.2 Experimental Methods

Scanning electron microscope (SEM, JSM-6510) and optical microscope (OM, OLYMPUS BX-51) were used to analyze the microstructure of the alloy. X-ray diffraction (XRD-7000, SHIMADZU Japan) uses an X-ray source: Cu-K α radiation coupling diffractometer at 200 mA and 40 kV continuous scanning. The 2 θ angle at which the samples were scanned ranged from 20° to 80° with 0.2° step size, and the collection time was 10 s. Rockwell hardness tester (HR-150A) was used to measure the hardness and test load: 150 kg. The digital microhardness tester (MICROMET-5103) was used to measure the micro-hardness, test load: 200 g and loading time: 10 s. In order to make sure the hardness data reproducibility, each sample had seven indentations under each experimental condition.

The wear test was carried out on the block-on-ring high-speed wear testing machine (MRH-3 W). GCr15 with hardness of 60–62 HRC (after quenching) was the grinding ring material, and the standard size was ϕ 40 mm \times 10 mm, and the composition was: 1.03C–0.35Mn–0.27Si–1.49 Cr (wt%) [14]. Test load was 294 N, and test wheel rotation speed was 200 r/min. Every test time was 120 min, and a 5-min alcohol ultrasonic cleaning and weighing were performed every 30 min. The different masses before and after the wear test were measured. TG328B balance was used to measure the weight loss, its weighing range was 200 g, and the accuracy was \pm 0.1 mg. The worn surface was observed by LEXT OLS 4100 laser confocal microscope and JSM6510 electron microscope.

3 Results and Discussion

3.1 As-Cast Microstructure of Fe–4Cr–B Alloy

Figure 1 represents the pseudo-binary vertical cross-sectional phase diagram of Fe–4Cr–xB alloy. It can be seen from Fig. 1 that when the B content is about 1 wt%, firstly with the decrease in the temperature, the crystallization reaction $L \rightarrow \delta\text{-Fe}$ occurs at 1395 °C, and the high-temperature ferrite precipitates directly from the liquid phase. As the temperature continues to decrease, the M_2B precipitates gradually. And the eutectic reaction $L \rightarrow \delta + M_2B$ occurs at 1283 °C, the liquid phase disappears at 1091 °C, and the coexistence region of $\delta + M_2B$ appears. Then, the $M_{23}C_6$ - and M_7C_3 -type carbides precipitate gradually. The final casting structure mainly is composed of $\alpha\text{-Fe}$, M_2B , M_7C_3 and $M_{23}C_6$.

Figure 2 shows the solidification structure of casting Fe–4Cr–B alloy, and it can be seen from the metallographic photograph shown in Fig. 2a that matrix and network eutectic phase are mainly composed of as-cast structure, and the eutectic phase is always distributed at grain boundary. As can be seen from the SEM image in Fig. 2b, a mixture of ferrite, martensite and lamellar pearlite is the main composition of the matrix. Figure 3 shows the X-ray diffraction analysis which shows that M_2B -, $M_7(C, B)_3$ - and $M_{23}(C, B)_6$ ($M = Fe, Cr, Mn$)-type borocarbides are the eutectic phase composition. Since B element’s solubility in $\gamma\text{-Fe}$ is 0.02%, which in $\alpha\text{-Fe}$ is 0.0004% [15], after the addition of boron element is excess,

it is mainly segregated at the grain boundary to form Fe_2B borocarbide. Because the atomic ratio of Cr to C is high, it is easy to form Cr_7C_3 during solidification. Besides the atomic size of Cr and Fe, and the arrangement of atoms of Cr_7C_3 and Fe_7C_3 are relatively close, a certain number of Fe atoms is replaced by Cr atoms and then forms $(Cr, Fe)_7C_3$ and $(Cr, Fe)_{23}(C, B)_6$. As can be seen from the SEM image and EDS line analysis of borocarbide in Fig. 4, Fig. 4a shows the eutectic boride skeleton and rod-like boride and grainy boride at the edge of grain. The line segment through various borides (Fig. 4b), and the EDS analysis results indicate that the Cr concentration in borocarbide is much higher than that in the other areas, while the C and Fe elements decrease in these areas. Since the C’s chemical composition in Fe can be reduced by Cr element, the formed borocarbide has relative stability [16, 17].

The surface scanning photographs of Fe–4Cr–B alloy show the EDS analysis of as-cast microstructure, which shows the distribution of elements in Fe–4Cr–B alloy; C and Cr are the main elements in the eutectic phase, as shown in Fig. 5. During solidification, when the eutectic reaction occurs, C and Cr elements form borocarbide, which is surrounded by some lean C and Cr regions [18], and these lean C and Cr regions will form a eutectic matrix. These two alternate reactions cause the eutectic structure a network structure. The Cr dissolved in the matrix has the effect of lowering the critical cooling rate of martensite, so a mixture of martensite and retained austenite is obtained during the cooling process. The

Fig. 1 The vertical sectional pseudo-binary phase diagrams of Fe–4Cr–xB alloy

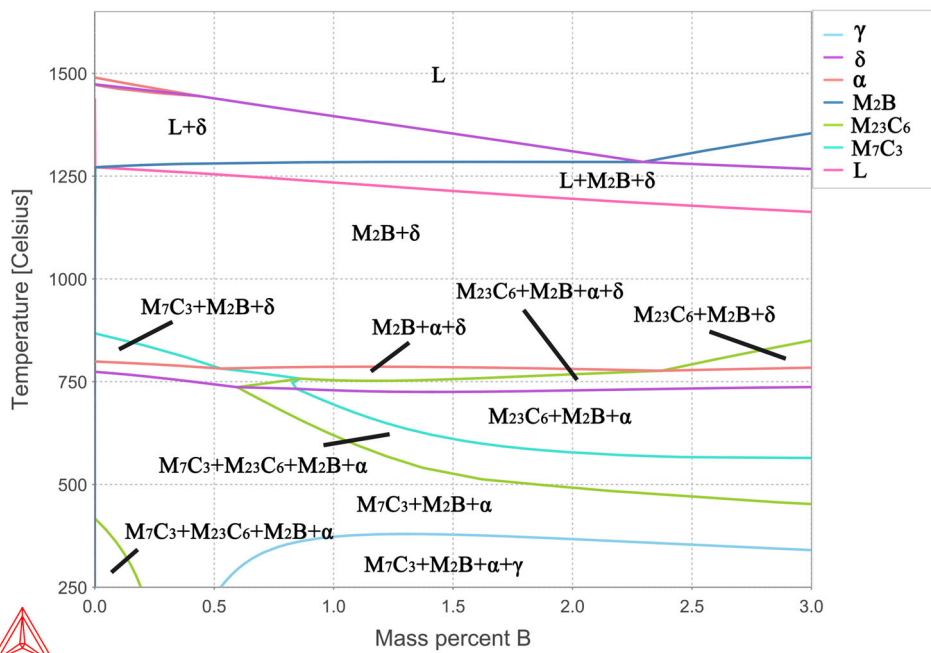
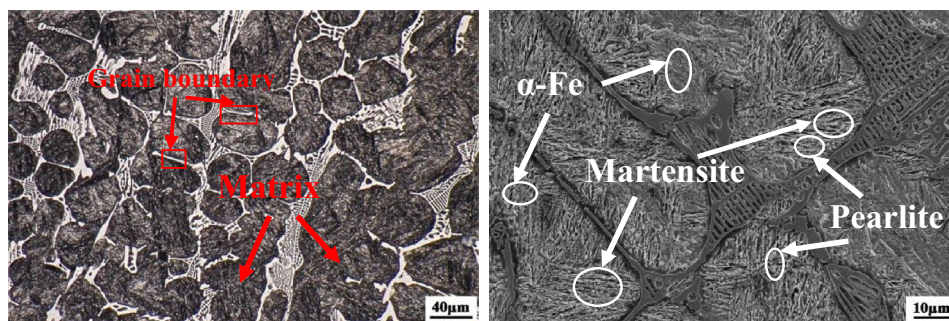


Fig. 2 Solidification structure of as-cast Fe–4Cr–B alloy



(a) OM photo

(b) SEM image

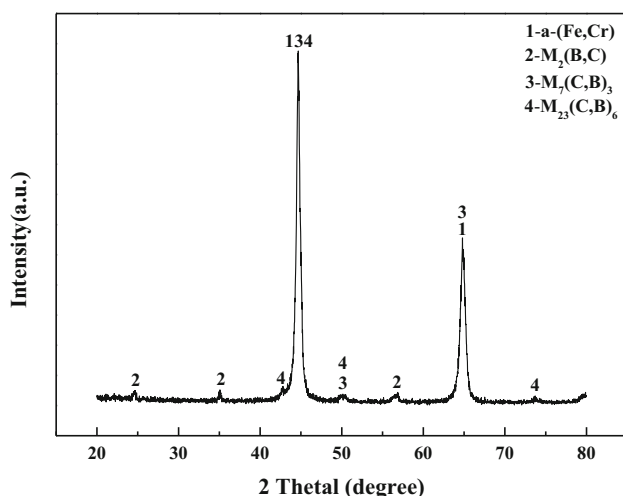
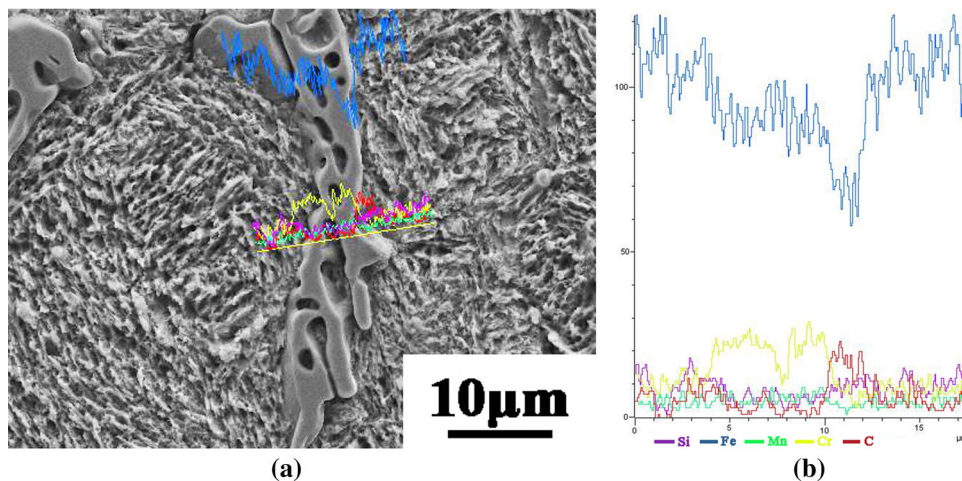


Fig. 3 The X-ray diffraction patterns of as-cast Fe–4Cr–B alloy

mainly distributed elements in the matrix are Fe and Si, and Si can be dissolved in the ferrite to increase the hardness of the matrix [16]. The Mn element is distributed in the eutectic structure and the matrix uniformly, without significant segregation.

Fig. 4 EDS line analysis of different regions in eutectic borocarbides



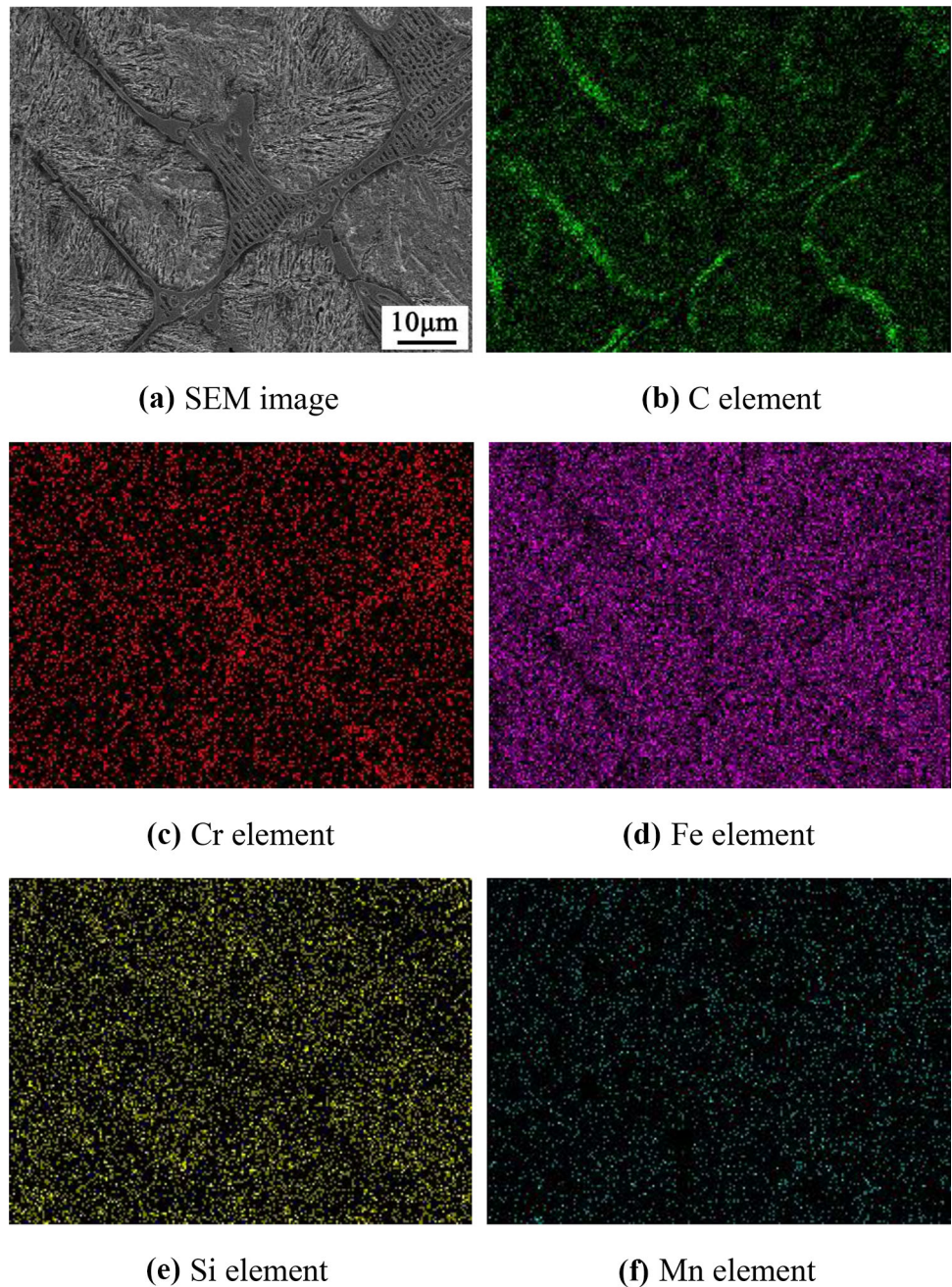
(a)

(b)

3.2 Effect of Water Quenching on Microstructure of Casting Fe–4Cr–B Alloy

Figures 6 and 7 show the OM and SEM images of the Fe–4Cr–B alloy whose water quenching temperatures are 950 °C, 1000 °C, 1050 °C, 1100 °C and 1150 °C. As shown in Fig. 6, after water quenching treatment at 950–1000 °C, the network structure of the eutectic phase has a tendency to break, and this phenomenon is distinct as the water quenching temperature increases to 1050–1100 °C, and the eutectic boride skeleton has a tendency to form an isolated distribution. This is because the quenching treatment promotes the M_2B (formed during solidification) which has high hardness and high brittleness to convert to a direction in which the surface free energy is reduced, B atoms diffuse into the matrix, and part of the eutectic borocarbide dissolves in the matrix, causing the network of the eutectic phase to break. The tendency of the phenomenon increases as the water quenching temperature increases, and it can be found that the sharp corners of the borocarbide become rounded, because the sharp corner of the borocarbide or the small weak point melts faster, and the crack often occurs in the weak place [19]. Since the crack is formed and it spreads on the brittle-hard

Fig. 5 Elemental distribution of eutectic borocarbides in Fe–4Cr–B alloy

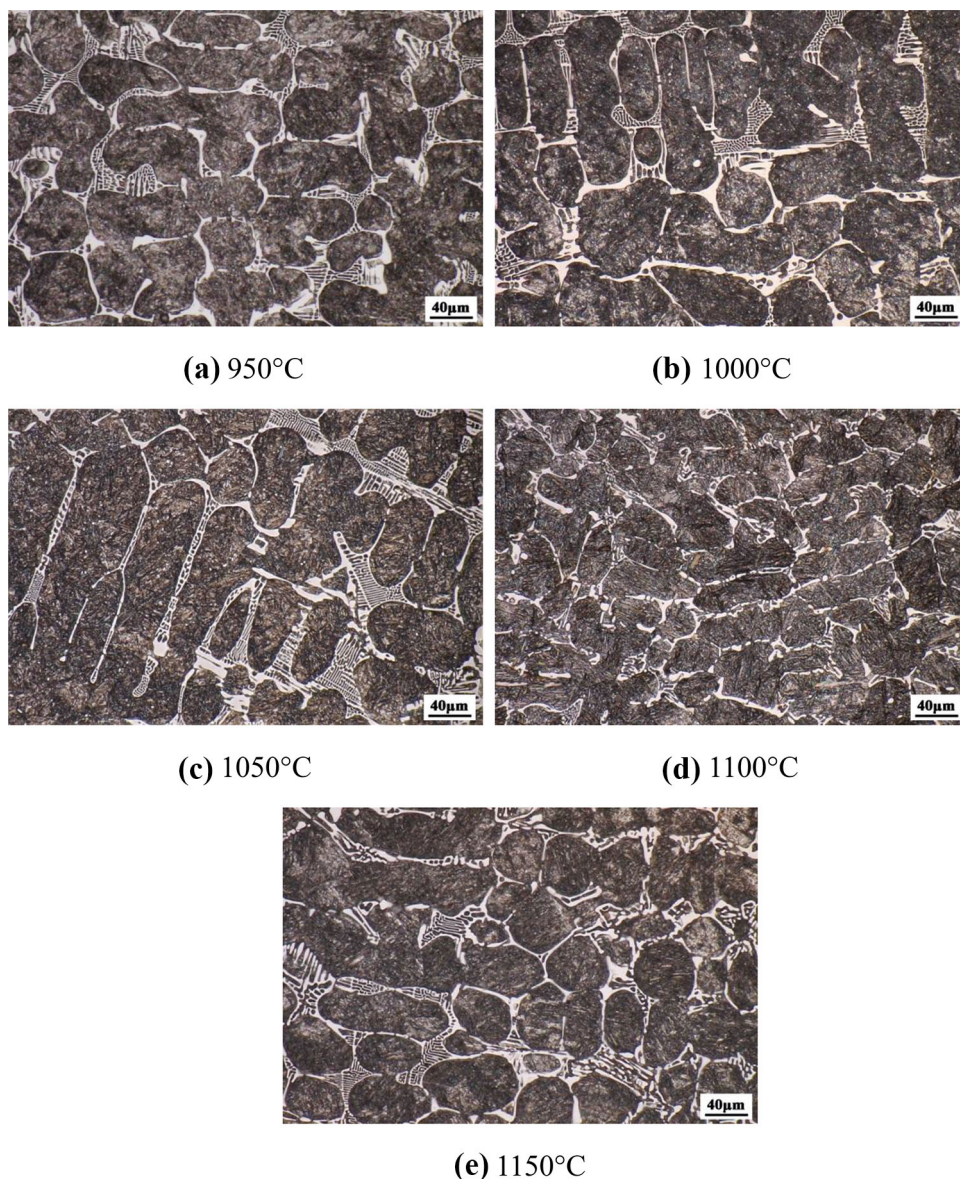


borocarbide phase, when the borocarbide around the matrix is in the form of a network, the crack propagation resistance is small and it easily breaks [20]. Therefore, it is a beneficial way to improve the toughness of casting Fe–Cr–B alloy to make the network structure of borocarbide fracture.

Figure 7 shows that the secondary borocarbides are in the form of short rod-like and grainy. Figure 8 shows the EDS point analysis of Fe–4Cr–B alloy quenched at 1100 °C, according to the atomic fraction ratio in Table 1, and the secondary borocarbides are short rod-like M_7C_3 and grainy $M_{23}C_6$. The XRD analysis of Fig. 9 shows the

effects of quenching temperature on the types and quantity of borocarbides, the calculation results of phase fraction can be found in Table 2, and it shows that as the quench temperature increases, the amount of ferrite in the matrix decreases, but that of martensite and secondary borocarbides increases. Because of the precipitation of secondary borocarbides during the quenching process, the content of alloying elements represented by chromium in the matrix is lowered, the stability of austenite is also reduced, the aging austenite is activated, and the M_s point is increased, which is favorable for forming martensite [16, 17]. As the water quenching temperature increases and reaches 1100 °C, the

Fig. 6 OM photographs of Fe–4Cr–B alloy quenched at different temperatures



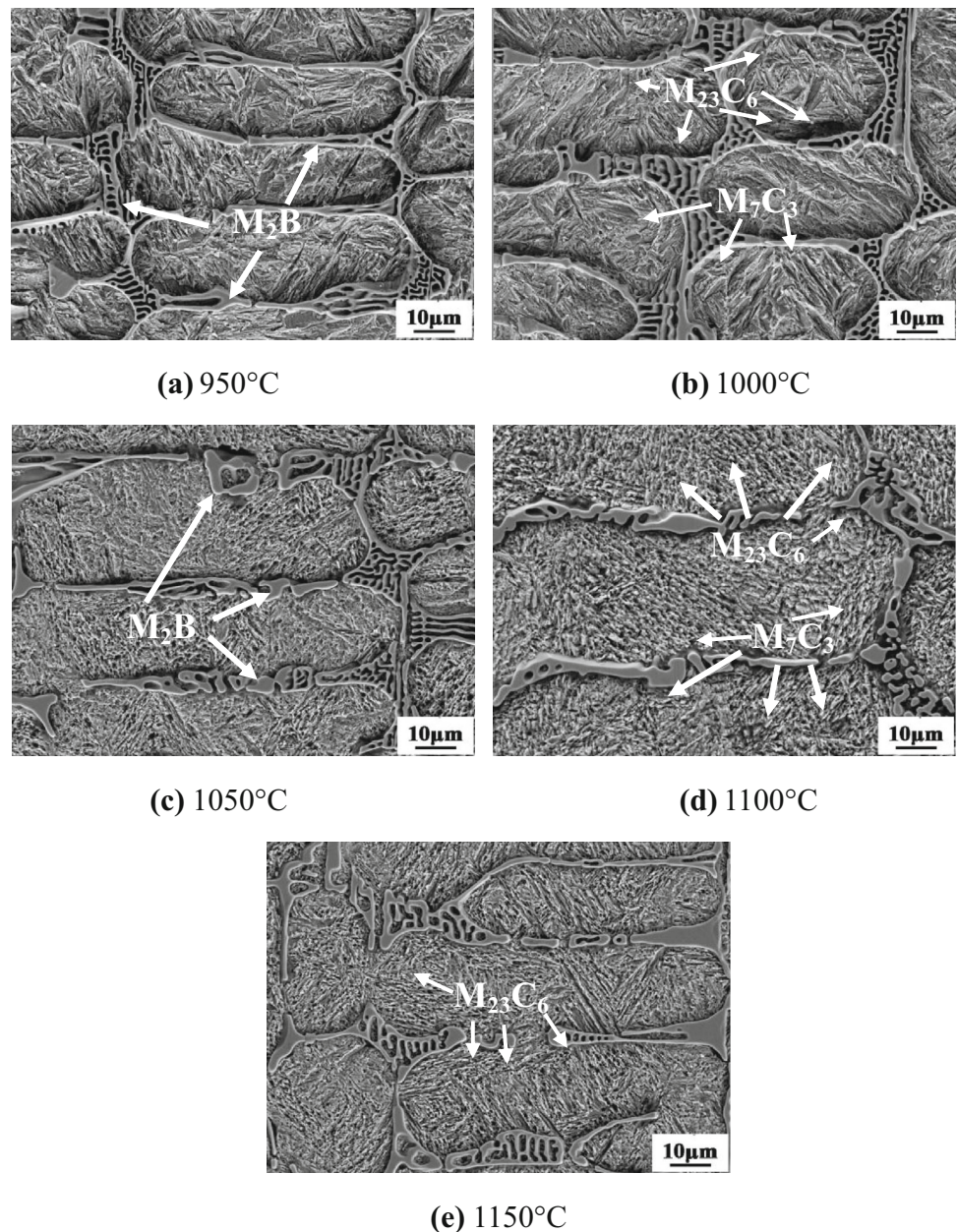
solid solubility of Cr and B elements in austenite increases, and the secondary borocarbides in the matrix re-decompose into the austenite, which enhances the stability of high-temperature austenite. The M_s point is lowered, and it is not easy to be transformed into martensite during water quenching, so that retained austenite reappears in the cooled structure.

Figure 10 shows the water quenching temperature effects on the macro-hardness and micro-hardness of the matrix. It can be seen from Fig. 10 that as the water quenching temperature increases, the macro-hardness of the alloy has an increasing tendency and reaches a maximum value of 62.8 HRC at 1100 °C. The macro-hardness and micro-hardness decrease slightly when the water quenching temperature exceeds 1100 °C. Because when water quenching temperature is low, pearlite cannot transform into austenite, the

quenched structure is still a mixture of pearlite (290–330 HV), ferrite (160–220 HV) and martensite (480–560 HV) [21] that lower the hardness of the matrix. As quenching temperature increases until it exceeds the austenite transformation temperature, when the quenching temperature increases, the amount of pearlite that transforms into austenite increases, and the micro-hardness of the matrix increases significantly as the proportion of martensite in casting Fe–4Cr–B alloy matrix increases.

Because the microstructure of the steel has an effect on the hardness of the alloy quenched, which is also affected by the saturated C, B and alloying elements in martensite and the remaining austenite [22]. Figure 11 shows the EDS composition scanning result of Fe–4Cr–B alloy quenched at 1100 °C, and the amount of C, B and alloying elements dissolved in the austenite is large (both over 9 wt%) when

Fig. 7 SEM images of Fe–4Cr–B alloy quenched at different temperatures



the water quenching temperature reaches 1100 °C, so the amount of saturated C, B and alloying elements in the transformed martensite is also large, and the number of precipitated secondary borocarbide increases, making the hardness relatively high; however, after reaching a certain water quenching temperature, as the temperature continues to increase, the remaining austenite in the quenched structure increases, resulting in a decrease in hardness. Therefore, it is an essential condition to ensure that a certain amount of C and alloying elements can be dissolved in the equilibrium austenite when selecting the quenching temperature of alloy, so that enough secondary borocarbides can precipitate to make the hardenability of the alloy strengthened. At the

same time, the increase in the amount of austenite that transforms into martensite can make the remaining austenite reduce and the hardness increase, quenching temperature of 1100 °C or less can avoid the transformation of the remaining austenite. Table 2 shows that the martensite transformation rate is the highest, reaching 24.65%, when water quenching temperature is 1100 °C.

3.3 Effect of Quenching on Wear Resistance of Casting Fe–4Cr–B Alloy

Wear resistance can be reflected by wear loss from the perspective of quantitative change, and the ratio of wear

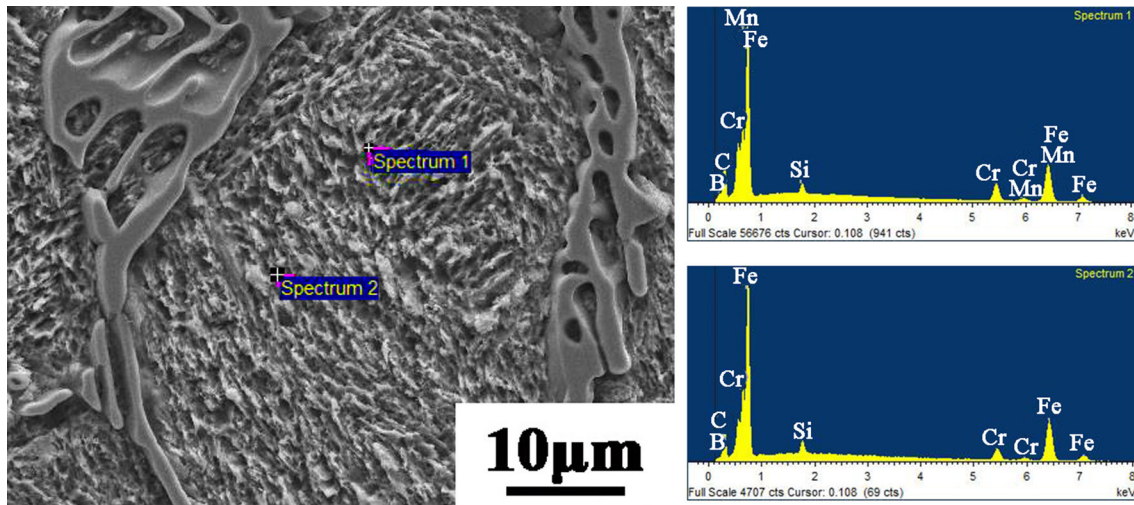


Fig. 8 EDS point analysis of different regions in eutectic borocarbides

Table 1 Chemical composition of different regions in secondary precipitation phase

EDS point	B		C		Si		Cr		Fe		Mn	
	wt%	at%	wt%	at%	wt%	at%	wt%	at%	wt%	at%	wt%	at%
Spectrum1	1.22	4.34	3.69	14.78	0.64	1.33	11.49	10.06	81.97	67.94	0.99	1.55
Spectrum2	3.24	14.07	4.53	15.45	0.97	1.42	15.59	12.15	75.68	56.92	–	–

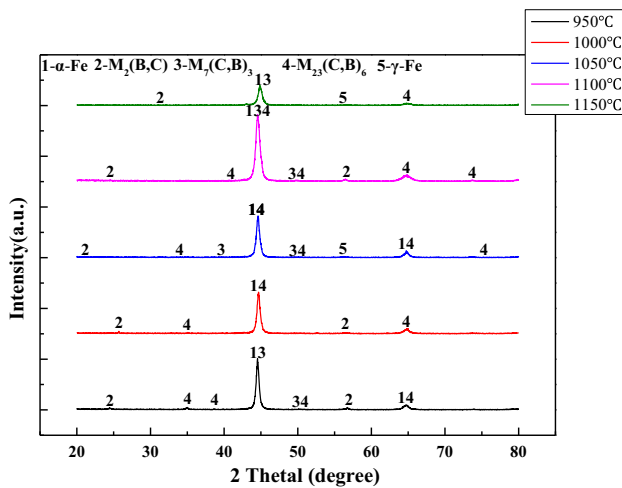


Fig. 9 X-ray diffraction pattern of Fe-4Cr-B alloy after water quenching

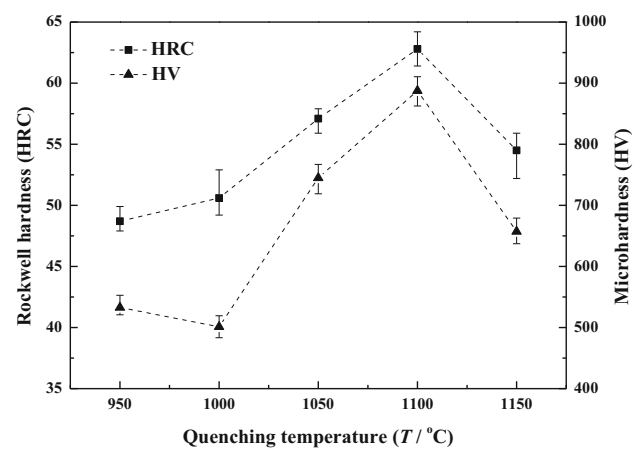
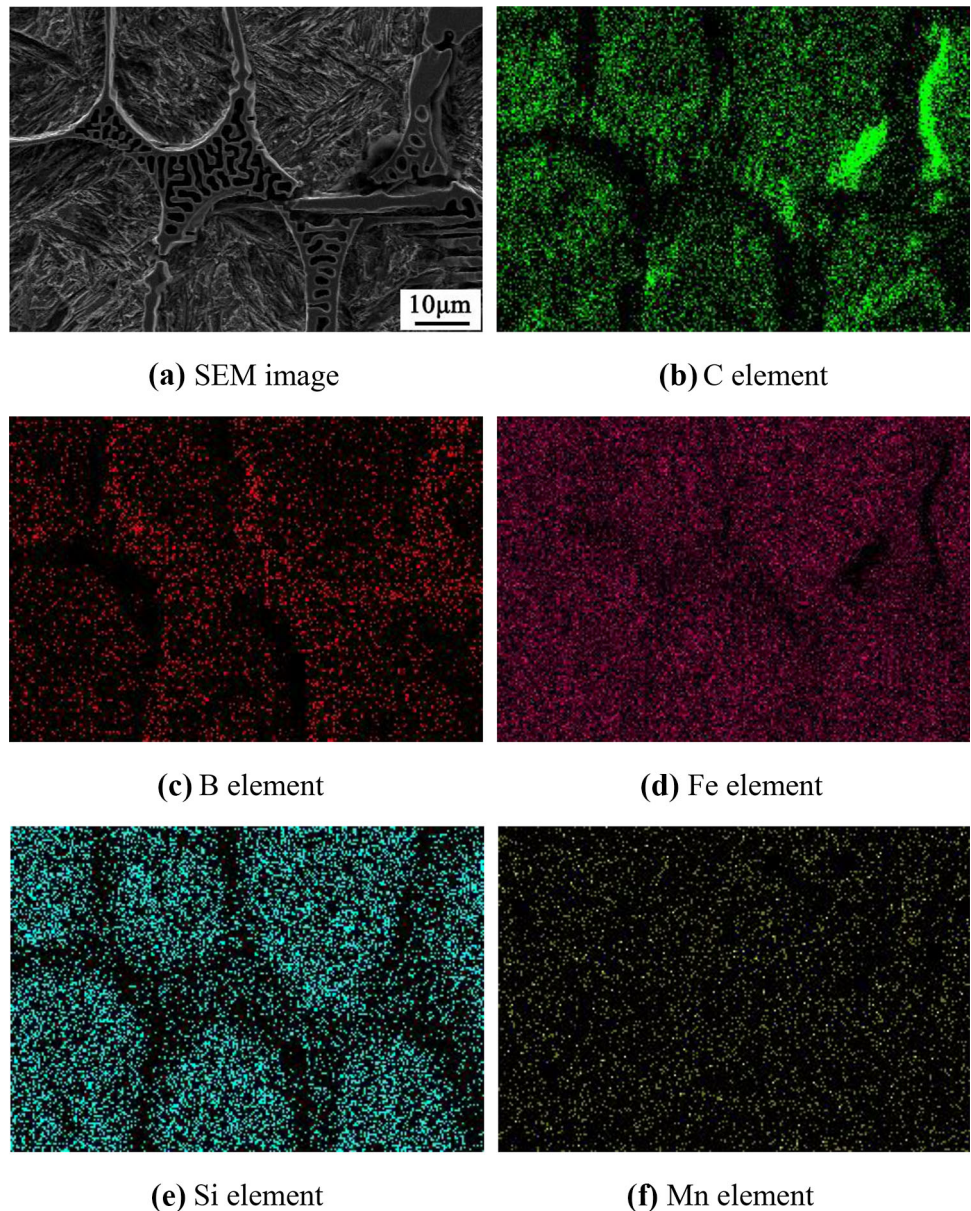


Fig. 10 Relationship between macro-hardness and micro-hardness with quenching temperature

Table 2 The volume fraction of matrix phase and borocarbide in the microstructure (vol%)

Sample	α -Fe	γ -Fe	Martensite	M_2 (B, C)	M_7 (C, B) ₃	M_{23} (C, B) ₆
As-cast	80.16	–	12.78	7.06	–	–
950 °C	69.36	–	16.32	6.98	2.23	5.11
1000 °C	73.46	–	14.54	7.02	–	4.98
1050 °C	61.16	5.78	22.36	6.84	–	3.86
1100 °C	57.02	–	24.65	5.28	5.73	7.32
1150 °C	49.55	14.29	23.15	6.92	2.98	3.11

Fig. 11 Elemental distribution of eutectic borocarbides in Fe–4Cr–B alloy quenched at 1100 °C



time and wear loss represents wear resistance. Figure 12 shows wear time effect on the wear loss. With the increase in the wear time, the wear loss of the alloy increases. Moreover, when the water quenching temperature is low, such as 950 °C and 1000 °C, the slope of wear loss and wear time curve of alloy is evidently larger than that of quenched alloy at 1050 °C and 1100 °C. Figure 13 shows the water quenching temperature effect on the wear loss and wear resistance of casting Fe–4Cr–B alloy. Wear loss of alloy shows a decreasing tendency as water quenching temperature increases initially and then increases, which is same as the changed trend of hardness. Besides, it can be seen from Fig. 13 that, at the temperature of 1100 °C, the wear loss is minimum, i.e., 12.1 mg, and the best wear

resistance is 9.92 min/mg, the worst wear resistance for the alloy quenched at 950 °C is only 3.39 min/mg, and its wear loss is as high as 35.4 mg. This is because, the resistance of alloy depends on its matrix structure and the size, shape, distribution and chemical composition of its hard phase [23]. The water quenching temperature directly affects the type, shape and quantity of the matrix and hard phase, which affects its wear resistance.

Further researches have been carried out by SEM to analyze the influence mechanism of the microstructure and wear resistance. Figure 14 shows its worn surface. From the images, we can see that the Fe–4Cr–B alloy experience severe deformation after wear at the water quenching temperature 900–950 °C. The worn surface had exfoliated

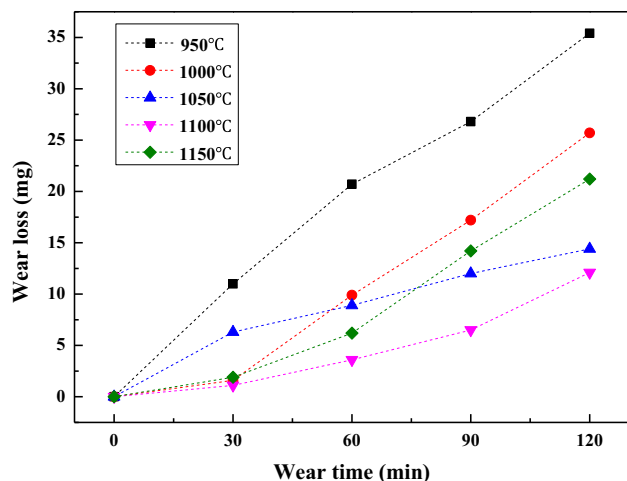


Fig. 12 Effect of wear time on wear loss of Fe-4Cr-B alloy after different quenching temperatures

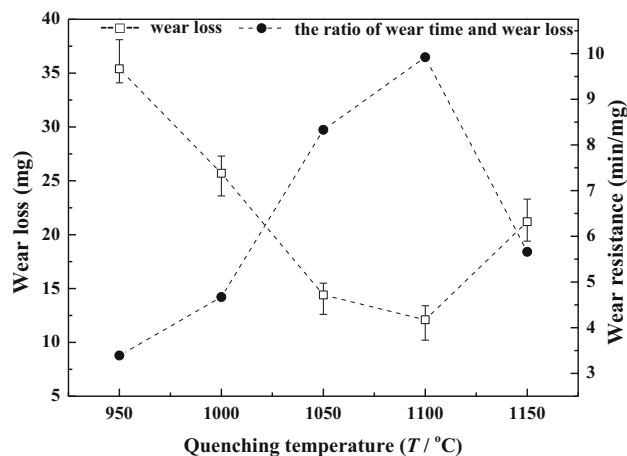


Fig. 13 Effect of quenching temperature on wear loss and wear resistance of Fe-4Cr-B alloy

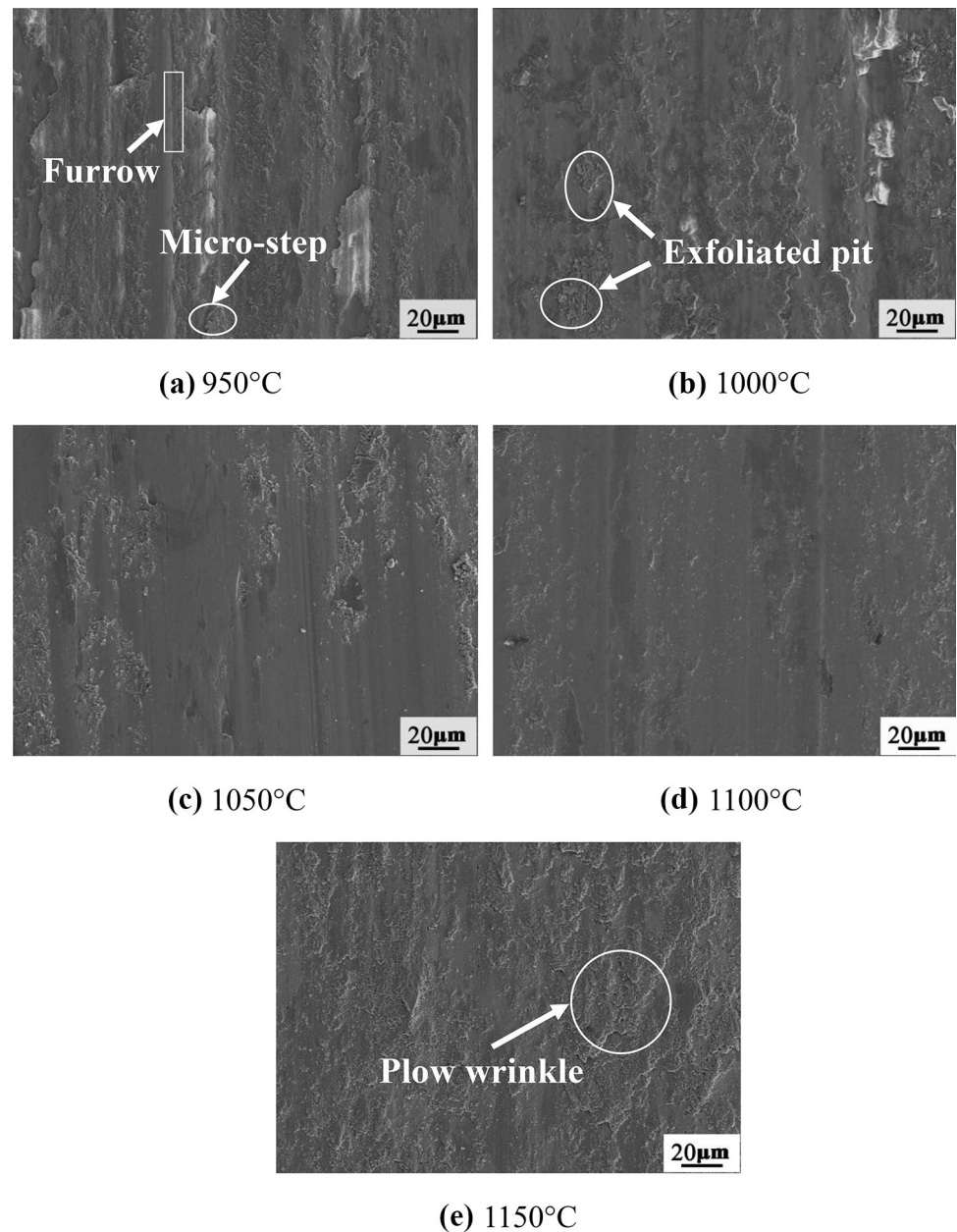
pits, plenty of furrows, plow wrinkles and micro-steps when the layers peel off. As the water quenching temperature increases, the depth of furrows in worn surface gradually decreases and turns shallow, and the exfoliated pits also fade away. But the worn surface will have deeper plow wrinkle when water quenching temperature exceeds 1100 °C. Figure 15 shows laser confocal photographs of the worn surface of Fe-4Cr-B alloy at different quenching temperatures, and the surface roughness analysis data are given in Table 3: S_q (root-mean-square height), S_a (the arithmetic average height) and S_z (maximum height) of Fe-4Cr-B alloy water-quenched at 1100 °C are all lower than those of other heat treatment temperatures, and at the same

time, the debris decreases and the worn surface become smooth. $S_{sk} > 0$ shows that the height distribution is below the average plane mostly, and the S_{ku} value shows the highly distributed needle-like sharp structure when quenching temperature is below 1000 °C or over 1100 °C. Both the matrix and borocarbides have an effect on the wear resistance. Based on the structure analysis, at the lower or higher water quenching temperature, ferrite, martensite and retained austenite are the main composition of the matrix structure, and its hardness is lower, while $M_2(B, C)$ phase hardness is relatively higher. At the beginning of wear, the matrix phase with lower hardness will be ground first and then the $M_2(B, C)$ phase with higher hardness will be exposed which will get worn in the following process. However, the low hardness of the matrix and its insufficient support to protect the $M_2(B, C)$ phase will cause the $M_2(B, C)$ phase to fall off and cause exfoliated pits. The high hardness $M_2(B, C)$ phase which is detached will cut off the matrix under the wear of the grinding ring during the wear process, which will result in a large number of deeper furrows and a poor wear resistance. When water quenching temperature is 1100 °C, the network borocarbides fracture. And the micro-hardness and hardness of the alloy are relatively high. The microstructure observation shows that the matrix and hard phase are well integrated, and they support and protect each other during the wear process. And because of the high hardness of the alloy matrix, the hard phase cannot be deeply pressed into the matrix. In the process of friction between the grinding ring and the grinding block, the larger hard phase will be ground, thus forming a small amount of abrasive debris and a shallow furrow.

4 Conclusions

- (1) Ferrite, pearlite, martensite and eutectic borocarbides are the main composition of the solidification structure of casting Fe-4Cr-B alloy. At the grain boundary, the eutectic borocarbides distribute in the form of a network and its type are M_2B , short rod-like $M_7(C, B)_3$ and grainy $M_{23}(C, B)_6$ ($M = Fe, Cr, Mn$).
- (2) Water quenching treatment makes the matrix changes to martensite, and secondary precipitation phases appears, the network eutectic phase has a fracture tendency, and there are no significant changes in grain size. As water quenching temperature increases, martensite conversion rate increases and reaches a

Fig. 14 SEM images of the worn surface of Fe–4Cr–B alloy at different quenching temperatures



maximum of 24.65% at 1100 °C, the volume fraction of $M_7(C, B)_3$ and $M_{23}(C, B)_6$ are 5.73% and 7.32%, respectively, and no austenite remains.

- (3) At water quenching temperature of 1100 °C, Fe–4Cr–B alloy has the minimum wear loss and the highest

wear resistance, because more secondary precipitation phase and harder martensite matrix support and protect each other during wear; at this time, the roughness of the worn surface is minimum ($S_a = 3.9 \mu\text{m}$).

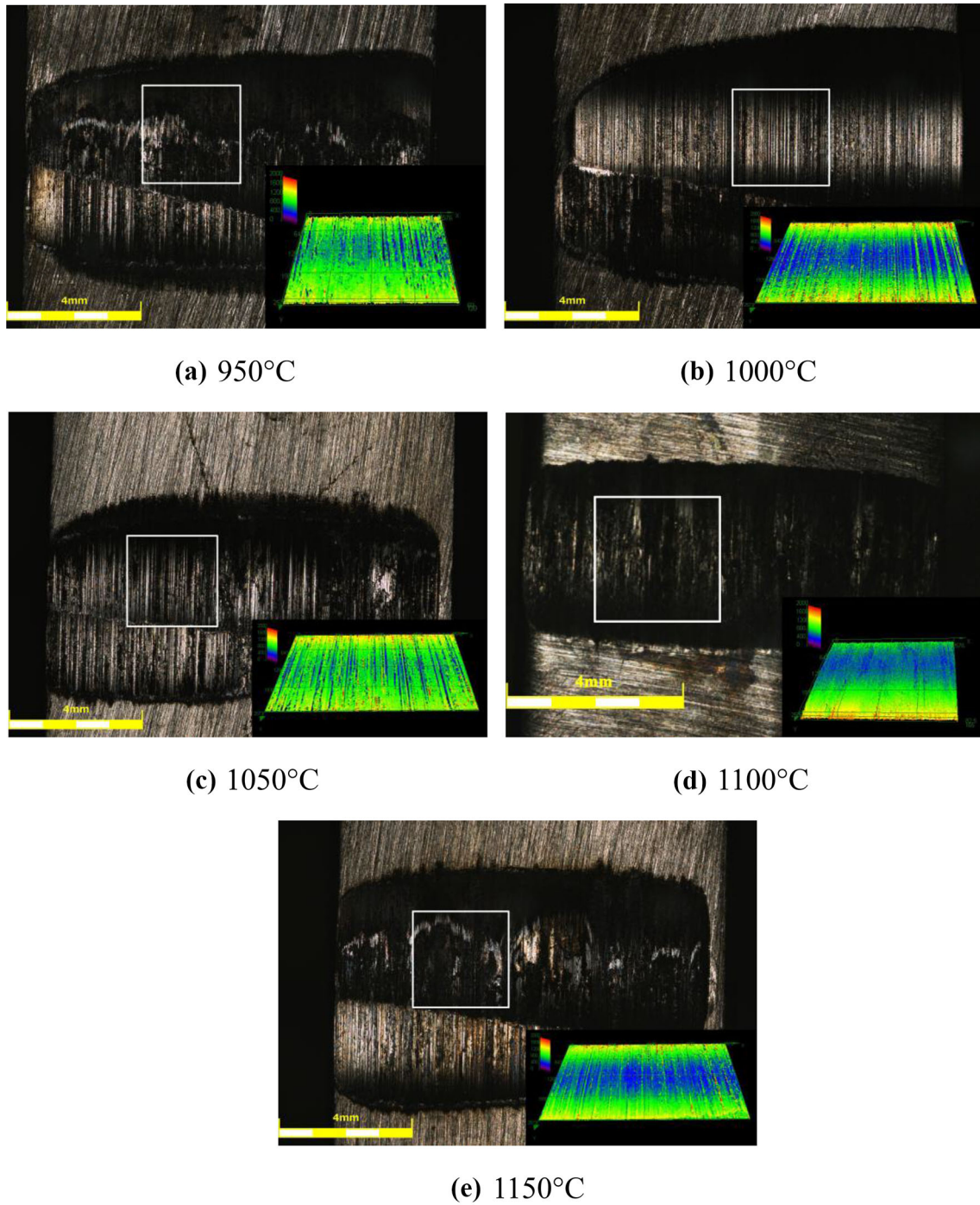


Fig. 15 Laser confocal photographs of the worn surface of Fe-4Cr-B alloy at different quenching temperatures

Table 3 Surface roughness measurement result of Fe-4Cr-B alloy after wear test

Sample [°C]	S_Q [μm]	S_{sk}	S_{ku}	S_p [μm]	S_v [μm]	S_z [μm]	S_a [μm]
950	19.9	0.35	10.62	209.9	203.2	413.1	13.3
1000	13.8	0.43	8.43	152.6	139.2	291.8	9.6
1050	27.1	0.10	8.33	224.3	185.5	409.7	18.1
1100	5.5	0.68	8.19	58.4	53.6	111.9	3.9
1150	16.5	1.23	15.68	207.9	183.7	391.7	10.7

Acknowledgements The authors would like to thank the financial support for this work from National Natural Science Foundation of China under grant (51775006) and Scientific Plan Item of Beijing Education Committee under Grant (009000546318529).

References

- Gou J, Lu P, Wang Y, Liu S, and Zou Z, *Appl Surf Sci* **360** (2016) 849.
- Nilsson A, Kirkhorn L, Andersson M, and Stahl J E, *Wear* **271** (2011) 1280.
- Lin C H, Komeya K, Meguro T, Tatami J, Abe Y, and Komatsu M, *J Ceram Soc Jpn* **111** (2003) 452.
- Wiengmoon A, Pearce J T H, and Chairuangri T, *Mater Chem Phys* **125** (2011) 739.
- Zhi X H, Liu J Z, Xing J D, and Ma S Q, *Mater Sci Eng A* **603** (2014) 98.
- Albertin E, Beneduce F, Matsumoto M, and Teixeira I, *Wear* **271** (2011) 1813.
- Zhang H, Fu H, Jiang Y, Guo H, Lei Y, Zhou R, and Cen Q, *Mater Sci Eng Technol* **42** (2011) 765.
- Christodoulou P, and Calos N, *Mater Sci Eng*, **A301** (2001) 103.
- Zhang J J, Gao Y M, Xing J D, Ma S Q, Yi D W, and Yan J B, *Tribol Lett* **44** (2011) 31.
- Yi D W, Xing J D, Ma S Q, Fu H G, Li Y F, Chen W, Yan J B, Zhang J J, and Zhang R R, *Tribol Lett* **45** (2012) 427.
- Yi Y L, Xing J D, Wan M J, Yu L L, Lu Y F, Jian Y X, *Mater Sci Eng A* **708** (2017) 274.
- Yüksel N, and Şahin S, *Mater Design* **58** (2014) 491.
- Cen Q, Zhang H, and Fu H, *J Iron Steel Res Int* **21** (2014) 532.
- Ju J, Fu H G, Fu D M, Wei S Z, Sang P, Wu Z W, Tang K Z, and Lei Y P, *Ironmak Steelmak* **45** (2018) 176.
- Hao S, *Modern Cast Iron*, Metallurgical Industry Press, Beijing (2009).
- Gu J, Fu H, Lei Y, and Ma S, *Mater Test* **57** (2015) 22.
- Ma S Q, Xing J D, Fu H G, Gao Y M, and Zhang J J, *Acta Mater* **60** (2012) 831.
- Wang S L, Cui L, He D Y, Zhou Z, and Jiang J M, *Hot Work Technol* **1** (2016) 30.
- Xiao-Le C, Jiang J, Yin-Hu Q, Li C, and Han-Guang F, *Trans Indian Inst Met* **71** (2018) 2261.
- Du Z Z, Li Y, Fu H G, Liu F, and Zhang H, *Trans Mater Heat Treat* **35** (2014) 50.
- Hanguang F, Xuding S, Yongping L, Zhiqiang J, Jun Y, Jinhua W, and Jiandong X, *Metals Mater Int* **15** (2009) 345.
- Fu H, Liu X, Yang Y, and Qu Y H *Trans Indian Inst Met* **71** (2018) 2423.
- Buchely M F, Gutierrez J C, León L M, and Toro A, *Wear* **259** (2005) 52.

Publisher's Note Springer Nature remains neutral with regard to jurisdictional claims in published maps and institutional affiliations.